Investigations into conformational transitions and solvation structure of a 7-piperidino-5,9-methanobenzo[8] annulene in water

ARTICLE *in* PHYSICAL CHEMISTRY CHEMICAL PHYSICS · NOVEMBER 2008

Impact Factor: 4.49 · DOI: 10.1039/b805505j · Source: PubMed

2 AUTHORS:

Natarajan Arul Murugan
KTH Royal Institute of Technology
72 PUBLICATIONS **574** CITATIONS
SEE PROFILE

Håkan Wilhelm Hugosson
KTH Royal Institute of Technology
30 PUBLICATIONS **701** CITATIONS
SEE PROFILE

Investigations into conformational transitions and solvation structure of a 7-piperidino-5,9-methanobenzo[8] annulene in water†

N. Arul Murugan* and Håkan Wilhelm Hugosson

Received 1st April 2008, Accepted 14th July 2008
First published as an Advance Article on the web 4th September 2008
DOI: 10.1039/b805505j

Solvation shell structure of a 7-piperidino-5,9-methanobenzo[8] annulene (PMA) in water has been investigated in ambient conditions using both molecular dynamics (MD) and Car-Parrinello molecular dynamics (CPMD) calculations. From the MD calculations, we find that this molecule exists in three major conformational states out of which two are in twist-boat forms and one in chair form. Due to the limited time scale accessible in CPMD simulations, we have studied all the three conformational states separately using CPMD. The molecular geometry, electronic charge distribution and solvation structure for all three forms are investigated. The stability order of the chair and twist-boat conformations in water solvent has been reversed when compared to the gaseous phase results and in the case of polar aprotic solvents (*J. Org. Chem.*, 1999, **61**, 5979). From the radial distribution function, we find that the solvent density around the chair form is significantly lower, which has to be directly related to the smaller solvent accessible area for this conformation and this is in complete agreement with earlier reports. Among the findings are that the solvation shell structure around the nitrogen atom in the chair form of PMA is considerably different from the open conformational forms or the twist-boat forms. The dipole moment for the closed form is found to be significantly larger when compared to the twist-boat forms.

1. Introduction

Cyclohexane or cyclopentane based organic compounds[1–3] and torsionally flexible molecules[4,5] are shown to exist in different conformational states. The relative population of different conformational states is decided by the solvents,[6,7] temperature, pressure and can also be modified by the chemical substitution of different groups.[3] In the case of steroids, the *trans*-axial arrangement of amine and hydroxyl groups destabilizes the chair conformation and stabilizes the twisted boat conformation.[8,9] Solvent dependent stabilization of different conformational states has also been reported for an androstanone derivative where the chair conformation is stabilized in a DMSO solvent and the twist chair conformation is stabilized by $CHCl_3$[9] solvent. The understanding of the structure and dynamics of conformationally flexible molecules is very important due to the potential use of these molecules as drug-delivery systems. But the modeling of these compounds poses difficulties due to unavailability of accurate and efficient force fields. A test for the efficiency of existing force fields is to correctly reproduce the molecular geometry and solvation structure for the flexible molecular systems. Therefore, we here provide a detailed study on the solvation dynamics of (5α,7β,8α,9α)–5,6,7,8,9,10-hexahydro-7-piperidino-5,9-methanobenzo[8] annulene (PMA) in water using both force-field based molecular dynamics[10] calculations and first-principles Car-Parrinello molecular dynamics (CPMD)[11,12] calculations. The candidate molecule has been experimentally studied in DMSO and chloroform solvents and the ^{1}H NMR and ^{13}C NMR spectra are reported at different temperatures.[13] Based on the NMR spectra, the solvent dependence and temperature dependence of different conformational states have been studied, reporting that PMA remains in two major conformational states in polar aprotic solvents (such as DMSO) with varying population. The reported conformational states[13] are the chair conformation and twist-boat conformation (see Fig. 1c and 1b, respectively) and the percentage populations of these two forms are 57 and 43%, respectively. The end-to-end distance for the twist-boat conformation is comparatively larger than the chair form. In the chair conformation, the hydroxyl and piperidine groups are in a *trans*-diaxial orientation and the piperidine ring is almost superimposed over the benzene ring. The equilibrium between these conformational states completely shifts towards the twist-boat (extended) form in $CDCl_3$ solvent.[13]

Previous molecular mechanics calculations on the chair and twist-boat conformational states have reported the molecular geometry and relative energies of these states.[13] The twist-boat conformer here being found to be higher in energy by 4 kcal mol^{-1} than the chair conformer. The solvent accessible area for the chair form is found to be significantly lower (by 26 Å^2) than that of the twist-boat form. The O–N distance is 2.82 Å in the case of the twist-boat form and it becomes 3.65 Å for the chair form. These calculations are static using a

Department of Theoretical Chemistry, School of Biotechnology, Royal Institute of Technology, SE-10691 Stockholm, Sweden.
E-mail: murugan@theochem.kth.se

† Electronic supplementary information (ESI) available: Molecular structure and labeling (Fig. S1); RESP and average D-RESP charges for PMA (Table S1); RESP and D-RESP charges for hydrogen atoms (Table S2); time evolution of total energy, volume and temperature of the system during the molecular dynamics run (Fig. S2). See DOI: 10.1039/b805505j

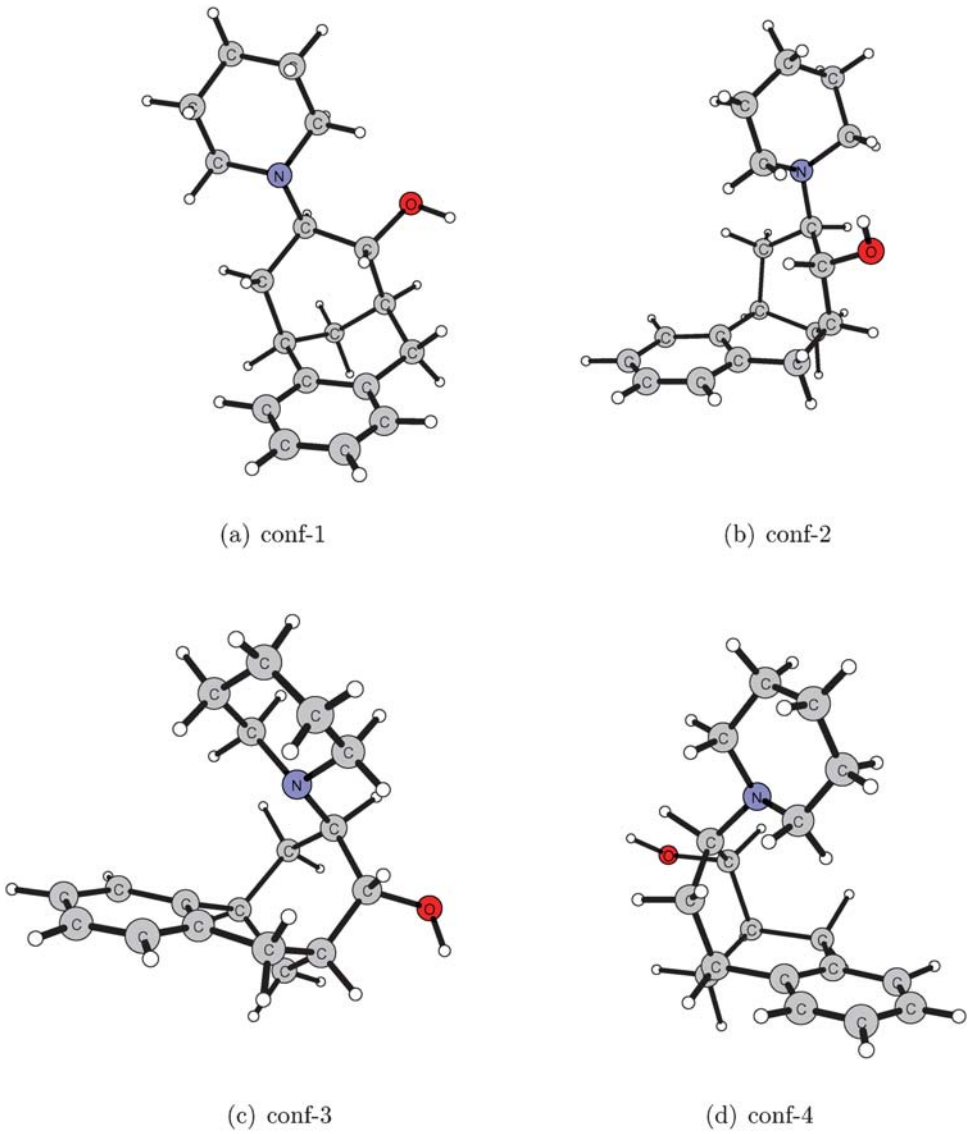

Fig. 1 Molecular geometry in different conformational states (a) conf-1 (b) conf-2 (c) conf-3 and (d) conf-4.

semi-empirical force field available in Chem-X software and the calculations were carried out for the molecule in a gaseous phase. So the temperature and solvent effects on the molecular geometry and solvation structure of PMA are completely missing in these studies. The present study therefore investigates the PMA molecule in a water solvent using both force-field based molecular dynamics calculations and CPMD calculations, focusing on the molecular geometry, electronic structure and solvation structure of different conformational states. Since the interconversion between different conformational states is a slow molecular process, the CPMD calculations are carried out for the (three) major conformational states found from the MD calculations. The solvation shell structure has been analyzed using various atom–atom radial distribution functions (rdf). The molecular geometry of PMA in its different conformational states has been analyzed using various molecular structural parameters. The average charges on various atomic sites and the average dipole moments are calculated for various conformational states.

2. Computational details

2.1 Molecular dynamics calculations

Earlier reported molecular mechanics calculations on the PMA molecule find that the chair form (see Fig. 1c) is stabler than the twist-boat form (Fig. 1b) by 4.0 kcal mol^{-1}.[13] So the molecule was initially prepared in the chair form and the structure optimized using a B3LYP functional and 6-31g(d,p) basis set in Gaussian03,[14] an *ab initio* electronic structure calculation software. The optimized structure was then solvated in 6658 water molecules in a cubic box using the xleap module of AMBER8.[16] The TIP3P model was used for water. The Shake algorithm[17] has been implemented to remove the highly mobile bond-stretching degree of freedom in water and the bond lengths are constrained to the equilibrium values. The generalized amber force field (GAFF)[15] has been used to model the atoms and interactions of the PMA molecule. The GAFF force-field provides a flexible molecular model for PMA with the torsional

degrees of freedom included. All MD calculations were carried out using the AMBER8 software.[16] Firstly, MD simulations were carried out at 300 K for PMA in water while keeping the molecule fixed in space. The total time length for this run was 100 ps. This allows the solvent structure around the PMA molecule to relax and equilibrate, avoiding the unphysical stabilization of the molecule by intramolecular hydrogen bonding before being fully solvated. Then the MD calculations were continued after removing the spatial constraint for the motion of the PMA molecule. The total time for this run was 9 ns with a time step for the integration of the equation of motion being 10 fs. A larger time step for integration has been chosen since the conformational transitions are usually considered to be rare events and to study the structure and dynamics of different conformational states one needs to have a relatively longer trajectory with the molecule spanning different states many times. Also the shake algorithm[17] implemented for water molecules allows us to select a relatively larger time step for integration. At the same time, we have made sure that a stable trajectory has been produced. The supplementary Fig. S1† shows the time evolution of total energy, volume and temperature of the system which clearly shows that a stable trajectory has been obtained with this time step for integration of the equation of motion. Here, we add a remark on the conservation of energy as we see in the subplot *a* of Fig. S1.† As we can see in the plot, the energy is conserved to 1 part in 1000 which is 10 times larger than the recommended value.[10] So, in order to produce a more accurate trajectory, we recommend a time step between 1–2 fs for simulation on flexible organic molecules. Since the water molecules are included explicitly in the solute–solvent system, we have used the dielectric constant value as unity. Simulations were run in a box with periodic boundary conditions and the particle mesh Ewald[18] method was used for treating electrostatic interactions. The cut-off distance for the direct summation employed is 10 Å.

2.2 Conformational transitions in PMA

The present molecular dynamics calculations report three major conformational states for PMA molecule in water instead of the two previously reported for the molecule in DMSO solvent. The nature of the conformational state, whether it is extended (twist-boat) or closed (chair), can be easily identified from the distance between the atoms C2 and C38 (see Fig. 2), here named R_{CC}, this being a measure of the end-to-end distance of the molecule. Fig. 3 shows the time evolution of the distance R_{CC}. Three regions can be seen here, with each domain associated with a specific conformational state. The chair form is the conformational state with a lower R_{CC} value, ranging between 3.5–6 Å. The twist-boat form then has a R_{CC} value above 6 Å. But here we find that the twist-boat form can exist in two conformational states, these two forms differing in the relative orientation of the piperidine ring and the cyclohexane ring. The conformation appearing between 7–9 Å is the one where the planes of the cyclohexane ring and the piperidine ring are parallel to each other. In the following discussion we will refer to this conformation as conf-1. The conformation where the planes of the cyclohexane ring and the piperidine ring are perpendicular to each other

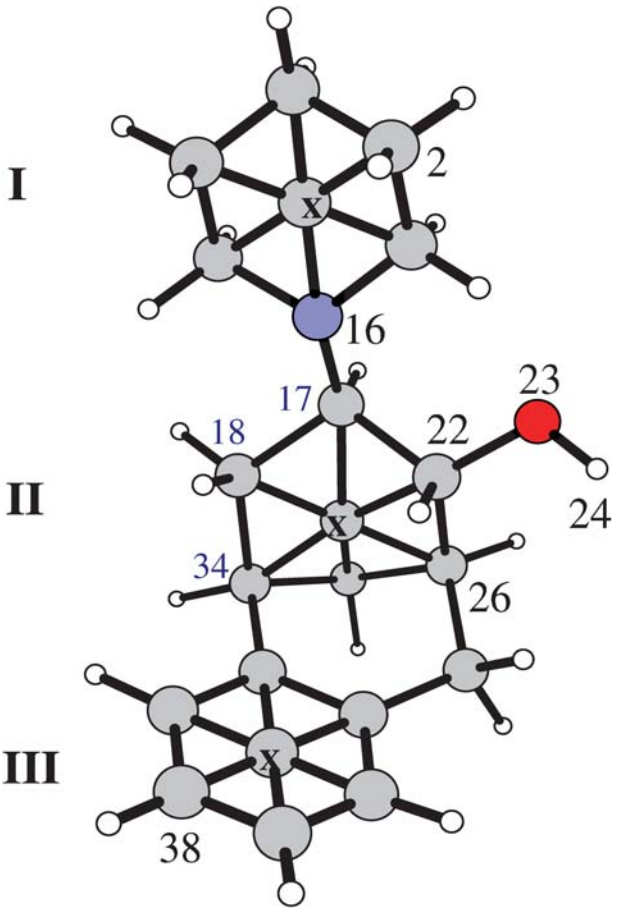

Fig. 2 Molecular structure for the PMA molecule and labeling of important atoms. In the figure I, II and III refer to the piperidine, unfused cyclohexane and benzene units of the molecule, respectively. The label × refers to the dummy atoms located at the center of these units.

has a R_{CC} value ranging between 6.3–7.8 Å, and will be referred as conf-2. For consistency, we will refer to the chair conformational state as conf-3. Earlier NMR calculations on PMA in DMSO report only conf-2 and conf-3.[13] In our calculations, we find conf-1 appearing as an intermediate during the interconversion between conf-3 and conf-2. The

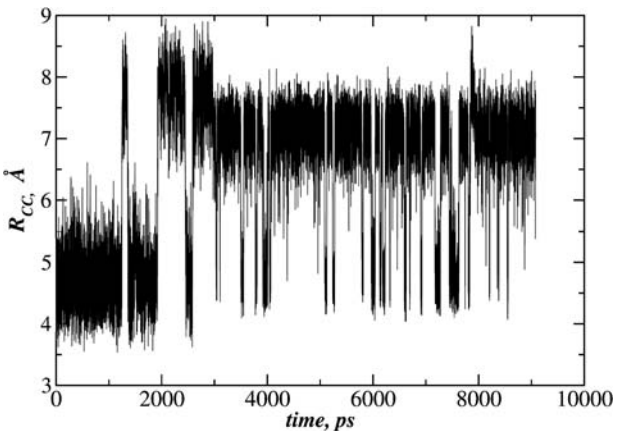

Fig. 3 Time evolution of R_{CC}, an end-to-end vector which shows different conformational states.

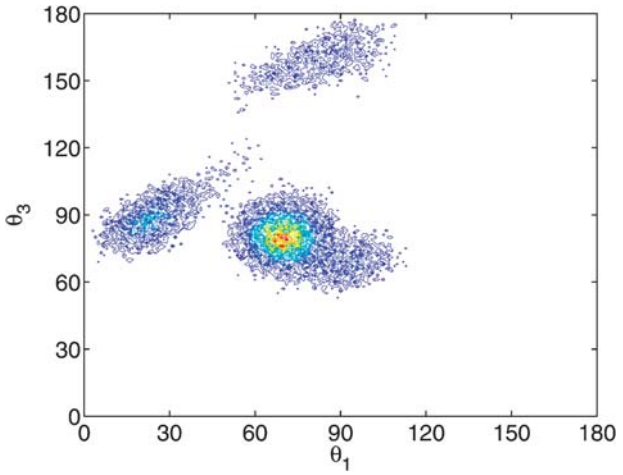

Fig. 4 Contour diagram of $f(\theta_1,\theta_3)$ which shows the relative orientation of the three six membered rings, namely, unfused cyclohexane ring, piperidine ring and benzene ring. Shown is the contour diagram calculated from the trajectory of MD calculations.

molecular geometries of conf-1, conf-2 and conf-3 are shown in Fig. 1a–c, respectively. We find that the relative orientations of three molecular subunits, namely piperidine ring, cyclohexane ring and benzene ring, can be used to distinguish between different conformational states. These three units are labeled as I, II and III in Fig. 2, respectively. The unit vectors $\hat{n}_1$, $\hat{n}_2$ and $\hat{n}_3$ are defined to be perpendicular to units I, II and III, respectively. The origin of the unit vectors is located at the site labeled as X in Fig. 2. And these three vectors define the orientation of all the three molecular subunits. Now, θ_1 is the angle between the vectors $\hat{n}_1$ and $\hat{n}_2$ and describes the relative orientation of the unfused cyclohexane ring and piperidine ring. Similarly, θ_3 is the angle between the $\hat{n}_1$ and $\hat{n}_3$ and describes the relative orientation of the piperidine ring and the benzene ring. Fig. 4 shows a contour diagram of $f(\theta_1,\theta_3)$ for the trajectory obtained from MD calculations. It shows clearly that there are three conformational states for PMA molecule in water. In this figure, conf-1 appears around $\theta_1 = 90^\circ$ and $\theta_3 = 165^\circ$, conf-2 around $\theta_1 = 75^\circ$ and $\theta_3 = 75^\circ$, and conf-3 around $\theta_1 = 0.0^\circ$ and $\theta_3 = 90^\circ$. The population density is represented in terms of color codes. With the change in color in the order blue, green, yellow to red, the density or population of states increases. This figure clearly shows that conf-2 and conf-3 are the most probable conformations, which can be related directly to their stability. The conf-1 seems to be relatively less stable than conf-2 and conf-3 but the population is still not negligible. Within conf-2 and conf-3, the population of conf-2 is much higher, which means the conf-2 is stabler than conf-3. So, based on the population of these three conformations, the stability appears in the order conf-2 > conf-3 > conf-1. It is interesting to compare the present case with the gaseous phase and with polar-aprotic solvents (DMSO). Based on the molecular mechanics calculations,[13] the order of stability for conf-2 and conf-3 has been reported to be conf-3 > conf-2 in the gaseous phase and the actual energy difference is 4 kcal mol^{-1}. In the case of polar aprotic solvents, the order appears to be the same again but the actual energy difference between conf-3 and conf-2 in DMSO is not reported. We find that our results are different from the findings in the gaseous phase and in the polar aprotic solvent. The difference being the population density of conf-3 is much larger compared to the reported 43% population in the case of DMSO. In order to estimate the correct energetics of different conformational states in the gaseous phase we have carried out the MP2 and BLYP calculations using the 6-311+G** basis set for three conformational states. The energetics are reported in Table 1. From both MP2 and BLYP level calculations, the conf-1 appears to be less stable. The MP2 level calculations predict the conf-3 is relatively stabler than conf-2 by 4.7 kcal mol^{-1}, with which the molecular mechanics calculations[13] results agree surprisingly. The BLYP level calculations predict comparably equivalent energetics for the conf-2 and conf-3. It is also important to remember that energetics and structure of different conformational states in different solvents can be quite different when compared to the gaseous phase energetics and structure.[19]

Table 1 BLYP/6-311+G** and MP2/6-311+G** level all-electron *ab initio* calculations based energetics for the three conformations

	BLYP		MP2	
System	E, H	Δ_E/kcal mol^{-1}	E, H	Δ_E/kcal mol^{-1}
Conf 1	−830.7273	3.65	−828.6739	8.56
Conf 2	−830.7331	0.0	−828.6800	4.71
Conf 3	−830.7325	0.37	−828.6875	0.0

2.3 Car-Parrinello molecular dynamics calculations

The density functional theory based Car-Parrinello molecular dynamics calculations were carried out for the three major conformations observed during the force-field molecular dynamics calculations. Three different conformational states were picked up from the MD calculation and the CPMD[20] calculations were carried out starting with each of these initial configurations. In our present calculations, we have used Becke, Lee, Yang and Parr (BLYP) gradient corrected functional[21,22] and the Troullier–Martins norm conserving pseudopotentials.[23] Here, the electronic wavefunctions were expanded in a plane wave basis set and the cutoff used was 80 Ry. We have used 5 au as the time step for the integration of the equation of motion and 600 amu as the fictitious electronic mass. The calculations were carried out in a QM/MM setup,[24] where the solute molecule (here it is the PMA molecule) is treated at an accurate density functional theory level while the solvents (water) are treated with a less accurate molecular mechanics force-field (TIP3P). The interaction between the QM and MM systems involves electrostatic, short range repulsion and long range dispersion interaction terms (using the empirical van der Waals parameters). The CPMD calculations involve the following three procedures: (1) quenching run: the electronic and ionic temperature of the initial structure is quenched to remove any hot spots in the system due to inaccurate molecular starting geometry; (2) scaled temperature run: a short run using temperature scaled dynamics done to bring the system to the required temperature and pressure; (3) Nose run: in this run, the system is kept to interact with a Nose-Hoover thermostat at the required temperature. The Nose thermostat mimics the real system

connected to a heat-bath to maintain the system temperature. The total time scale for the CPMD calculations is 4–5 ps.

3. Results and discussions

3.1 Molecular geometry of PMA in different conformations

Here, we discuss the molecular geometry of the PMA molecule in different conformations using some of the important structural parameters: (1) $f(\theta_1,\theta_3)$, where θ_1 is the angle between the unfused cyclohexane ring and the piperidine ring while θ_3 is the angle between the piperidine ring and the benzene ring; and (2) the N–O bond length; (3) hydrogen bonding geometry and (4) ϕ_{OH}, being the dihedral angle that defines the conformation of the hydroxyl group. Fig. 5a–c show the position of conf-1, conf-2 and conf-3, respectively, in the contour plot of $f(\theta_1,\theta_3)$. The molecular geometry for the conf-2 and conf-3 obtained from the force-field molecular simulations appear to be similar to the geometry obtained from CPMD calculations. Conf-1 spans a larger space in θ_3 when compared to its classical analogue, suggesting that the classical force-field describing this degree of freedom is much steeper. In other words, the CPMD calculations predict a much flatter potential energy profile for the angular rotation of the piperidine ring in the axial position of the twist boat cyclohexane ring. Fig. 6a and b show the N–O bond distribution for different conformational states obtained from MD and CPMD calculations, respectively. The average NO bond distances are reported in Table 2 and compared to the earlier static calculations[13] reported for this molecule. The NO bond distance for the chair form is comparably higher than the bond-distance of twist-boat forms in all calculations. Gratifyingly, the NO bond distance calculated from MD calculations and CPMD calculations for both conf-1 and conf-2 is almost equivalent. There is a difference of 0.04 Å for the MD and CPMD calculated NO bond distance of conf-3. The NO bond distance calculated from molecular mechanics calculations was low for both conf-2 and conf-3 when compared to the MD and CPMD calculated bond lengths. Fig. 7 shows the geometry of the hydrogen bonding between the OH group of the PMA molecule and the oxygen atom of the water molecule. Fig. 7a shows the hydrogen bonding geometry obtained from the MD trajectory, while Fig. 7b–d show the hydrogen bonding geometry obtained from the CPMD trajectories for conf-1, conf-2 and conf-3, respectively. In the MD trajectory the average

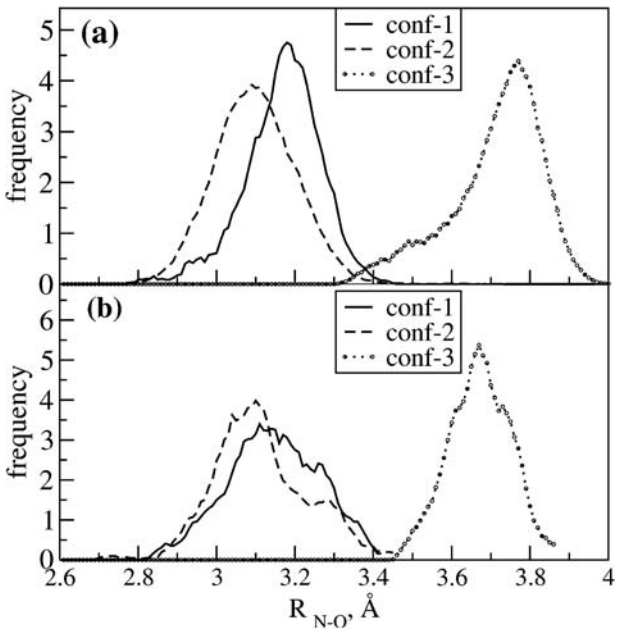

Fig. 6 The distribution of NO distance for different conformations obtained from (a) MD calculations and (b) CPMD calculations.

Table 2 Average NO bond distances

System	Static	Amber	CPMD
Conf 1	—	3.17	3.15
Conf 2	2.82	3.10	3.10
Conf 3	3.65	3.71	3.67

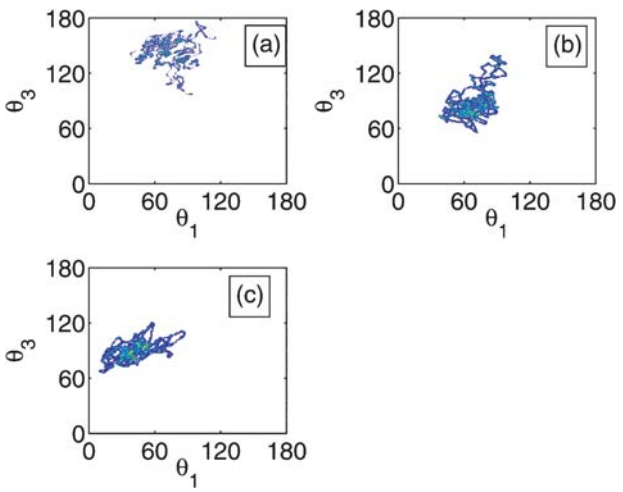

Fig. 5 Contour diagram of $f(\theta_1,\theta_3)$ obtained from the CPMD calculations separately for three different conformational states. (a) conf-1 (b) conf-2 (c) conf-3.

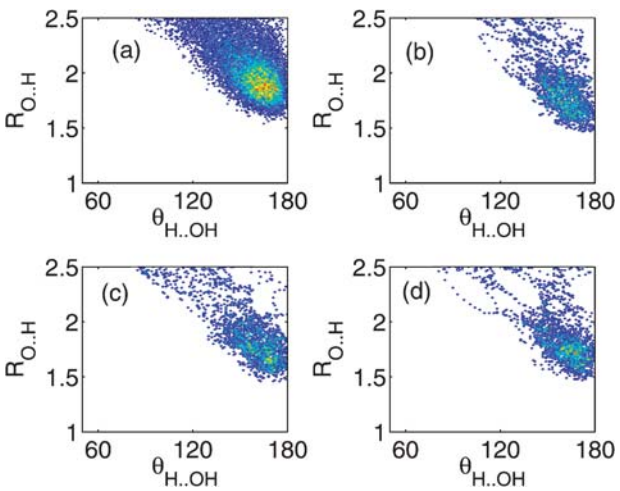

Fig. 7 Hydrogen bonding geometry obtained from MD calculations and CPMD calculations. The subplot (a) has been obtained from the MD trajectory and the subplots (b), (c) and (d) are obtained from the CPMD trajectory for conf-1, conf-2 and conf-3, respectively.

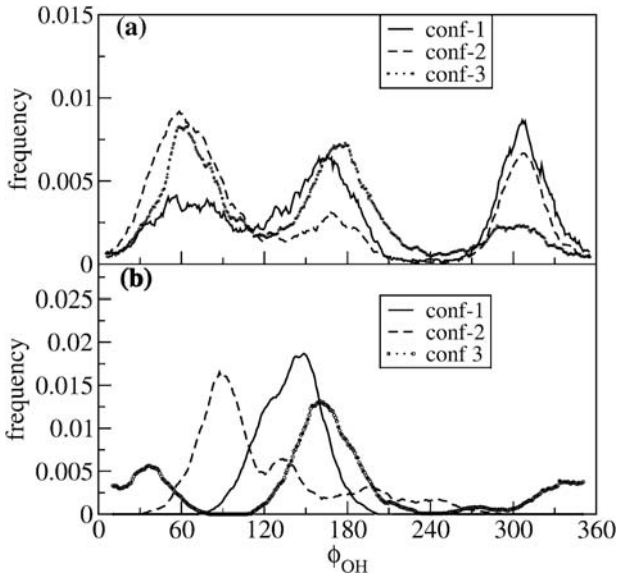

Fig. 8 The distribution of ϕ_{OH} calculated from (a) the MD trajectory and (b) the CPMD trajectory. The distribution function has been computed for conf-1, conf-2 and conf-3 separately.

hydrogen bonding geometry has the parameters $\theta_{H\cdots OH}$ = 170° and $R_{O\cdots H}$ = 1.80 Å. The hydrogen bonding for the all the conformations appears to be more or less similar. When compared to MD calculations, the $R_{O\cdots H}$ parameter of the hydrogen bonding from the CPMD appears at a lower value of R, which is close to 1.6 Å. A hydrogen bonding with this geometry is usually characterized as 'strong' hydrogen bonding in the literature.[25,26] The CPMD calculations show that the hydrogen bonding geometry is not altered significantly due to change in the conformation in the case of the PMA molecule.

3.2 Conformational mobility of the hydroxyl group

In this section, we will discuss the conformational mobility of the hydroxyl group of the PMA molecule calculated using MD and CPMD calculations. The conformational mobility of the hydroxyl group can be discussed using the distribution of the dihedral angle, ϕ_{OH} which describes the relative orientation of the hydroxyl group with the cyclohexane ring. Here, ϕ_{OH} which is the dihedral angle between the atoms H24–O23–C22–C26. Fig. 8a shows the dihedral angle distribution calculated from the MD trajectory. It appears that the molecule has three minimum energy conformations appearing at dihedral angles ϕ_{OH} = 60, 180 and 300°. The barriers for the torsional interconversion appear at the dihedral angles 0, 120 and 240°. The three curves in Fig. 8a shows the conformation dependence of the population of the ϕ_{OH}. Even though the three peaks appear in all three curves, one peak is relatively lower in height. The position of the peak with a smaller amplitude appears at different angles for the three conformational states. It is interesting to note that, depending on the molecular conformation, the potential energy profile for the torsional motion of the hydroxyl group changes. Fig. 8b also displays the dihedral angle distribution calculated for three conformational states but from the CPMD trajectory. We see considerable difference in the distribution of ϕ_{OH} when compared to MD results. We see a multimodal behavior in the distribution of ϕ_{OH} for conf-2 and conf-3 and not for conf-1. This clearly shows the hydroxyl group in conf-1 undergoes a small-amplitude torsional motion. If we analyze the molecular geometry of conf-1, this can be explained easily. In conf-1, the hydroxyl group is located sterically closer to the hydrogen atoms connected to C3 (the carbon between C2 and N; see Fig. 2). The steric repulsion from these hydrogen atoms does not allow the hydroxyl group to undergo free torsional interconversion. In the case of conf-2 and conf-3, the ϕ_{OH} distribution displays a relatively larger conformational mobility for the hydroxyl group. The peak positions for the maximum in the distribution appear at slightly different angles when compared to the results obtained from MD calculations. Due to the relatively smaller time scale accessible to CPMD, the peak positions will be dependent on the initial structure.

3.3 Charge distribution and dipole moments of PMA

In this section, we will discuss the charge distribution and dipole moments of the PMA molecule in different conformations. The force-field MD calculations use fixed charge for the atomic sites to model the electrostatic interactions. But it is known that the charge distribution is often strongly dependent on the molecular conformation.[27] So it is important to know how much the atomic charges and dipole moments can change for different conformations. Here, we get dynamical restrained ESP (D-RESP)[28] charges from CPMD calculations and these atomic charges are generated from the best-fitting of point charges to reproduce the molecular electrostatic potential of the charge density. Depending upon the environment and molecular conformation, the D-RESP charges evolve as a function of time. Tables S1 and S2 of the ESI† give the average D-RESP charges of the heavy and light atoms, respectively. For comparison, the charges used in the force-field MD calculations are also displayed in the tables (usually static RESP charges). For many of the atoms, the RESP charges are larger in magnitude. The D-RESP charges for conf-1 and conf-2 appear to be mostly equivalent. However, a remarkable difference is seen in the case of the nitrogen atom, where conf-1 and conf-2 have a −0.2 electronic charge, while the conf-3 has a much lower atomic charge, close to zero. This is easily explained since in conf-1 and conf-2 the N atom is involved in hydrogen bonding with the solvent water molecules, and is therefore more negatively charged. The distribution of atomic charges for the N atom and OH group for all three conformers is shown in Fig. 9a and b, respectively. This figure clearly shows that the atomic and group charges in a molecule are considerably changed by the conformation. The distribution curves for conf-1 and conf-2 appear to have a single peak, while for conf-3 the distribution curve has two peaks. In order to understand this we have plotted the time evolution of the charges on the nitrogen atom and the hydroxyl group, which is shown in Fig. 10a and b, respectively. Interestingly, the time evolution of the nitrogen charges for conf-1 and conf-2 remain constant with significant fluctuation around this value. However the time evolution of conf-3 remains constant for up to 4100 fs and beyond this shows a sudden increase in magnitude. After this jump in magnitude, the charge again fluctuates around a

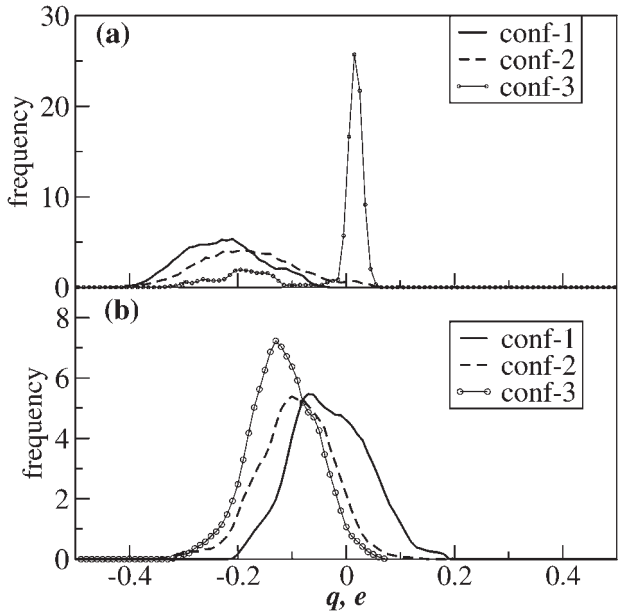

Fig. 9 (a) Charge distribution of the nitrogen atom of the PMA molecule and (b) the charge distribution of the hydroxyl group. The charge distribution function has been computed for conf-1, conf-2 and conf-3 separately.

constant value. When we analyzed the time evolution of molecular geometry, we find that the conf-3 undergoes a conformational transition to a structure as shown in Fig. 1d. Interestingly, this structure is different from conf-1 and conf-2. This conformer (referred to as conf-4 from here onwards) appears closer to conf-2 in terms of $f(\theta_1,\theta_3)$ which means that the relative orientations of the three rings (as shown in Fig. 2) are similar to conf-2. The difference in the geometry between conf-2 and conf-4, is due to the dihedral angle between the atoms C34–C18–C17–N16 which is −166 and −107° for conf-4 and conf-2, respectively. Another interesting aspect is the

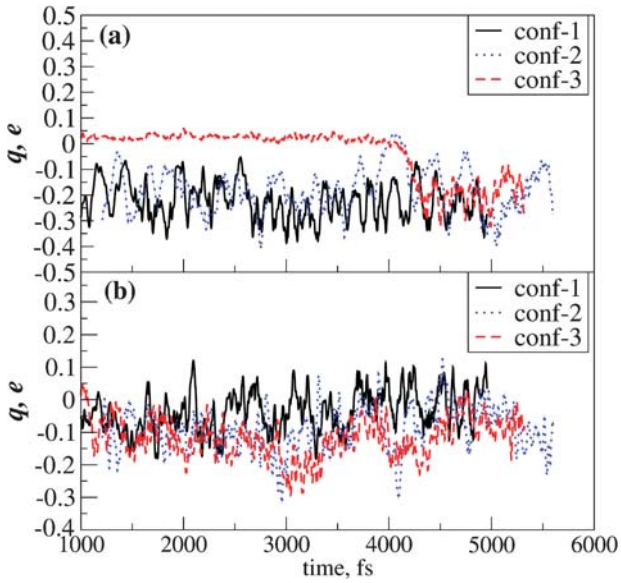

Fig. 10 Time evolution of charges of (a) the nitrogen atom and (b) the hydroxyl group for different conformational states.

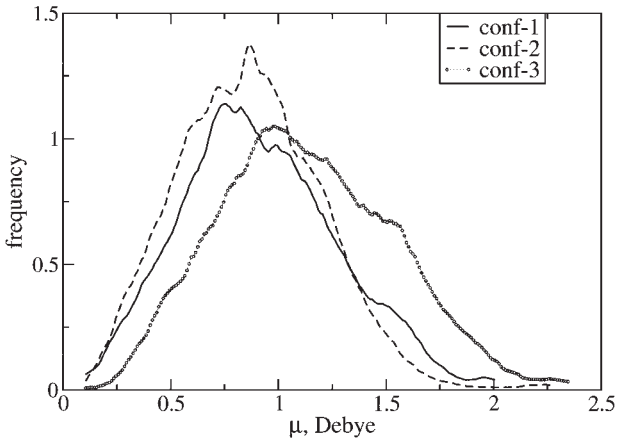

Fig. 11 Dipole moment distribution for PMA in its different conformational states.

fluctuation in the charge of the N atom in all four conformational states. The charge of the N atom in conf-3 fluctuates the least, which should be attributed to the conformational rigidity of this form. Usually, the DRESP charge fluctuation is due to the change in the internal molecular geometry as well as due to the change in the solvent environment. In the case of conf-3, the molecule almost behaves like a rigid molecule and the fluctuation we see is just due to the change in solvent environment. Fig. 11 shows the dipole moment distribution for all the three conformations. The average dipole moments are 0.91, 0.87 and 1.13 au for conf-1, conf-2 and conf-3, respectively. Conf-3 has a relatively larger dipole moment when compared to other conformers. Due to the large dipole moment of conf-3, one may expect larger stabilization of this conformer than other conformer in a more polar solvent like water. However, our calculations show that this is not the case. So, there may be other factors such as the solvent accessible area that determine the stability of a conformer in a solvent. As has been reported,[13] conf-3 has a less solvent-accessible area which directly leads to lower solute–solvent interactions. This could be the reason for the lower stability of the conf-3, in water. Investigations into the solvation dynamics of PMA in DMSO and the chloroform solvents using MD and CPMD calculations are in progress which may shed more light into the stabilization/destabilization of different conformers in polar aprotic and non-polar solvents.

3.4 Solvation shell structure

In this section, we discuss the solvation structure of PMA in water calculated from MD and CPMD. The solvation structure can be easily understood in terms of different solute-solvent rdfs. Fig. 12 shows the rdfs such as $g_{\text{X-com}}(r)$, $g_{\text{O-com}}(r)$ and $g_{\text{N-com}}(r)$ calculated from the trajectory obtained from MD calculations. Here, the label X refers to all atoms in the PMA molecule and com refers to the center of mass of the water molecules. The first peak appearing below 2.24 Å in $g_{\text{X-com}}(r)$ is due to the hydrogen bonding between the hydroxyl group of the PMA molecule and the water oxygen atom. From the plots, it can be clearly seen that the solute has an influence on the solvent structure up to a distance of around 8 Å, beyond which the bulk density is equal to one. The density of water appears to be significantly lower around the

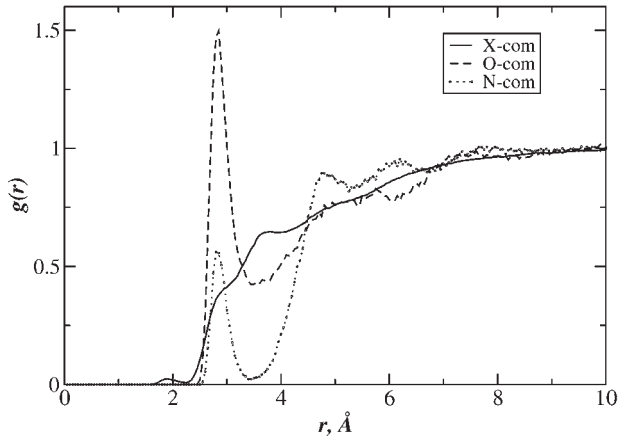

Fig. 12 Various radial distribution functions, namely, $g_{X\text{-com}}(r)$, $g_{O\text{-com}}(r)$ and $g_{N\text{-com}}(r)$ calculated for the trajectory obtained from MD calculations.

PMA molecule. There exists a clear structure around N and O atoms of the PMA, which can be seen from the well-defined first peak in the $g_{O\text{-com}}(r)$ and $g_{N\text{-com}}(r)$ rdfs. Even though the number of N and O atoms is the same (one in PMA molecule) the average coordination number of water molecules around these atoms differs significantly. We will see in the later part of the text that this is due to the masking of the N atom in the chair conformation. The molecule exists in dynamic equilibrium between the different conformations, where the conformations have a different coordination number around the N atom and hence the average coordination number of the N atom is lower than that of the O atom. Fig. 13 displays the rdfs for the different conformations calculated from the CPMD calculations. The rdfs such as $g_{X\text{-com}}(r)$, $g_{O\text{-com}}(r)$ and $g_{N-com}(r)$ are presented for different

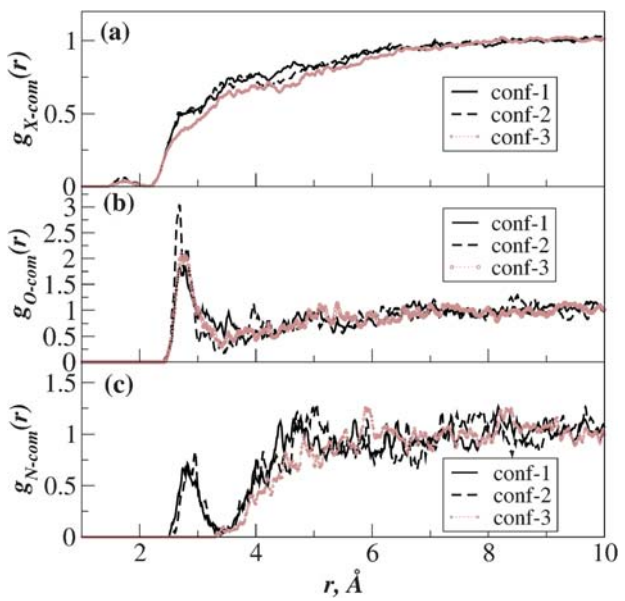

Fig. 13 Various radial distribution functions, namely, $g_{X\text{-com}}(r)$, $g_{O\text{-com}}(r)$ and $g_{N\text{-com}}(r)$ for the three conformational states calculated for the trajectory obtained from CPMD calculations. The subplots (a), (b) and (c) show the radial distribution functions calculated for conf-1, conf-2 and conf-3, respectively.

conformations in Fig. 13a–c, respectively. The appearance of the first peak in $g_{X\text{-com}}(r)$ (with $r > 2$ Å) for all three conformations shows that intermolecular hydrogen bonding exists in all three conformations. However there exists a remarkable lowering of the height in $g_{X\text{-com}}(r)$ of conf-3 up to 6 Å. The lowering of the peak height is directly related to the appearance of a lower number of solvents around conf-3 when compared to other conformational states. This has its origin in the lower solvent accessible area of conf-3, as has already been reported.[13] The $g_{O\text{-com}}(r)$ curve for all three conformational states appears to be the same suggesting the solvation structure around the oxygen atom is similar in all the states. The $g_{N\text{-com}}(r)$ of conf-1 and conf-2 are seen to be very similar and therefore the solvation structure around the N atom is the same in the case of conf-1 and conf-2. The first solvation shell appears between 2.5–3.5 Å. However there exists a marked difference in $g_{N\text{-com}}(r)$ of these two conformations and that of conf-3 in terms of the first solvation shell structure. There is a complete disappearance of the first solvation structure in the case of conf-3 which arises from the masking or inaccessibility of the N atom to the water solvents.

5. Conclusions

Investigation here into the solvation structure of the PMA molecule in water solvents using MD calculations report three major conformational states for the solute molecule. These conformational states differ in the relative orientations of the benzene, cyclohexane and piperidine rings. The so-called chair form differs with the other two twist boat forms in terms of solvation shell structure. The nitrogen atom is masked/buried in the chair form and is therefore unavailable for solvation. The atomic charge on the nitrogen atom in the chair form is closer to zero and is considerably different to the charge on the nitrogen atom in other conformational states. The dipole moment of the chair form is relatively higher compared to the twist-boat forms.

Acknowledgements

The authors acknowledge Prof. Hans Ågren and PDC for access to computational facilities. Authors also acknowledge the Wenner-Gren foundation for financial support. This work was supported by a grant from the Swedish Infrastructure Committee (SNIC) for the project "Multiphysics Modeling of Molecular Materials", SNIC 023/07-18.

References

1 M. Squillacote, R. S. Sheridan, O. L. Chapman and F. A. L. Anet, *J. Am. Chem. Soc.*, 1975, **97**(11), 3244.
2 W. Cui, F. Li and N. L. Allinger, *J. Am. Chem. Soc.*, 1993, **115**, 2943.
3 V. Madison and D. Kopple, *J. Am. Chem. Soc.*, 1980, **102**, 4855.
4 N. A. Murugan, *J. Chem. Phys.*, 2005, **123**, 094508.
5 N. A. Murugan and S. Yashonath, *J. Phys. Chem. B*, 2004, **108**, 17403.
6 S. Madurga and E. Vilaseca, *J. Phys. Chem. A*, 2004, **108**, 8439.
7 C. Cappelli, S. Corni and J. Tomasi, *J. Phys. Chem. A*, 2001, **105**, 10807.
8 l. Fielding and G. H. Grant, *J. Am. Chem. Soc.*, 1991, **113**, 9790.
9 l. Fielding and G. H. Grant, *J. Am. Chem. Soc.*, 1993, **115**, 1902.

10 M. P. Allen and D. J. Tildesley, in *Computer Simulation of Liquids*, Oxford University Press, USA, June 29, 1989.
11 R. Car and M. Parrinello, *Phys. Rev. Lett.*, 1985, **55**, 2471.
12 W. Andreoni and A. Curioni, *Parall. Comput.*, 2000, **26**, 819.
13 L. Fielding, J. K. Clark and R. McCuire, *J. Org. Chem.*, 1996, **61**, 5978.
14 M. J. Frisch, *et al.*, *GAUSSIAN 03 (Revision B.01)*, Gaussian, Inc., Wallingford, CT, 2004.
15 J. Wang, R. M. Wolf, J. W. Caldwell, P. A. Kollman and D. A. Case, *J. Comput. Chem.*, 2004, **25**(9), 1157.
16 D. A. Case, T. E. Cheatham III, C. L. Simmerling, J. Wang, R. E. Duke, R. Luo, K. M. Merz, B. Wang, D. A. Pearlman, M. Crowley, S. Brozell, V. Tsui, H. Gohlke, J. Mongan, V. Hornak, G. Cui, P. Beroza, C. Schafmeister, J. W. Caldwell, W. S. Ross and P. A. Kollman, AMBER8, University of California, San Francisco, CA, 2004.
17 J.-P. Ryckaert, G. Ciccotti and H. J. C. Berendsen, *J. Comput. Phys.*, 1977, **23**, 327.
18 T. Darden, D. York and L. Pedersen, *J. Chem. Phys.*, 1993, **98**, 10089.
19 C. M. Backer and G. H. Grant, *Chem. Commun.*, 2006, **13** 1387.
20 J. Hutter, M. Parrinello, D. Marx, P. Focher, M. Tuckerman, W. Andreoni, A. Curioni, E. Fois, U. Roetlisberger, P. Giannozzi, T. Deutsch, A. Alavi, D. Sebastiani, A. Laio, J. VandeVondele, A. Seitsonen and S. Billeter, Computer code CPMD, version 3.11, Copyright IBM Corp. and MPI-FKF Stuttgart 19902002.
21 A. D. Becke, *Phys. Rev. A: At., Mol., Opt. Phys.*, 1988, **38**, 3098.
22 C. Lee, W. Yang and R. C. Parr, *Phys. Rev. B: Condens. Matter Mater. Phys.*, 1988, **37**, 785.
23 N. Trouiller and J. L. Martins, *Phys. Rev. B: Condens. Matter Mater. Phys.*, 1991, **43**, 1993.
24 P. Carloni, U. Rothlisberger and M. Parrinello, *Acc. Chem. Res.*, 2002, **35**, 455.
25 G. R. Desiraju and T. Steiner, *The Weak Hydrogen Bond in Structural Chemistry and Biology*, Oxford University Press, Chichester, 1999.
26 G. A. Jeffrey, *An Introduction to Hydrogen Bonding*, Oxford University Press, New York, 1997.
27 C. A. Reynolds, W. Jonathan, W. J. Essex and W. G. Richards, *J. Am. Chem. Soc.*, 1992, **114**, 9075.
28 C. I. Bayly, P. Cieplak, W. D. Cornell and P. A. Kollman, *J. Phys. Chem.*, 1993, **117**, 5179.